Journal of Rock Mechanics and Geotechnical Engineering 14 (2022) 93–107

Contents lists available at ScienceDirect

Journal of Rock Mechanics and Geotechnical Engineering

journal homepage: www.jrmge.cn

Full Length Article

Effects of amygdale heterogeneity and sample size on the mechanical properties of basalt

Zhenjiang Liu [a], Chunsheng Zhang [b], Chuanqing Zhang [c,d,*], Huabin Wang [a], Hui Zhou [c,d], Bo Zhou [a]

[a] School of Civil and Hydraulic Engineering, Huazhong University of Science and Technology, Wuhan, 430074, China
[b] PowerChina Huadong Engineering Corporation Limited, Hangzhou, 310014, China
[c] State Key Laboratory of Geomechanics and Geotechnical Engineering, Institute of Rock and Soil Mechanics, Chinese Academy of Sciences, Wuhan, 430071, China
[d] University of Chinese Academy of Sciences, Beijing, 100049, China

ARTICLE INFO

Article history:
Received 13 January 2021
Received in revised form
18 July 2021
Accepted 18 October 2021
Available online 19 November 2021

Keywords:
Amygdaloidal basalt
Hard brittle rock
Structural heterogeneity
DFN-FDEM
Mechanical properties
Size-dependent effect

ABSTRACT

Due to the complex diagenesis process, basalt usually contains defects in the form of amygdales formed by diagenetic bubbles, which affect its mechanical properties. In this study, a synthetic rock mass method (SRM) based on the combination of discrete fracture network (DFN) and finite-discrete element method (FDEM) is applied to characterizing the amygdaloidal basalt, and to systematically exploring the effects of the development characteristics of amygdales and sample sizes on the mechanical properties of basalt. The results show that with increasing amygdale content, the elastic modulus (E) increases linearly, while the uniaxial compressive strength (UCS) shows an exponential or logarithmic decay. When the orientation of amygdales is between 0° and 90°, basalt shows a relatively pronounced strength and stiffness anisotropy. Based on the analysis of the geometric and mechanical properties, the representative element volume (REV) size of amygdaloidal basalt blocks is determined to be 200 mm, and the mechanical properties obtained on this scale can be regarded as the properties of the equivalent continuum. The results of this research are of value to the understanding of the mechanical properties of amygdaloidal basalt, so as to guide the formulation of engineering design schemes more accurately.

1. Introduction

As a natural geological material, discontinuous structures of various scales are widely developed inside rock mass, ranging from microcracks and holes at a mesoscale to joints and fissures at a macroscale, and even faults up to several hundred metres long. At a small scale, the existence of such high heterogeneity significantly affects the mechanical properties of rock, and at a large scale, it directly controls the safety and stability of the entire engineering rock mass. It has been accepted that brittle rock failure is often a dynamic evolution process from continuous to discontinuous, in which these native defects are constantly going through crack closure, initiation, propagation, and coalescence under the action of loading, eventually causing macroscopic fracture of the material (Esmaieli et al., 2010; Liu et al., 2018).

Consequently, laboratory tests and numerical simulations were used to investigate the influences of holes, cracks, and other defects on the fracture evolution, deformation and strength of rocks and rock-like materials. A variety of factors influencing rock failure mechanism, including the mechanical (unfilled or filled and type of filling) and geometric (shape, length, quantity, and orientation) properties of defects, and stress conditions have been analysed (Jin et al., 2017; Aziznejad et al., 2018; Cao et al., 2018; Wang et al., 2018; Shaunik and Singh, 2019; Yang et al., 2018; Zhou et al., 2018; Zhang et al., 2020). Research has suggested that the key contribution of defects is acting as stress concentration mechanism capable of producing tensile stress concentration at the tip of microcracks, resulting in local damages and failure of the samples. Hence, defects play a key role in brittle rock failure.

Considering the existence of discontinuities at various scales, the mechanical properties of a specific rock, such as strength and

* Corresponding author. State Key Laboratory of Geomechanics and Geotechnical Engineering, Institute of Rock and Soil Mechanics, Chinese Academy of Sciences, Wuhan, 430071, China.
E-mail address: cqzhang@whrsm.ac.cn (C. Zhang).
Peer review under responsibility of Institute of Rock and Soil Mechanics, Chinese Academy of Sciences.

https://doi.org/10.1016/j.jrmge.2021.10.001

deformation, exhibit a certain scale-dependence. Hoek and Brown (1980) analysed laboratory test data and proposed an empirical size-effect formula in a normalised form, in which the uniaxial compressive strength (UCS) for rock samples with any diameter is related to that of rock samples of 50 mm in diameter. The synthetic rock mass method (SRM) is based on the numerical simulation that combines a discrete fracture network (DFN) model representing discontinuities with conventional numerical models representing the complete matrix, which can fully consider the scale and anisotropy effects of the characteristics of rock masses (Vöge et al., 2013; Zhang et al., 2015; Yang et al., 2017; Zhou et al., 2018, 2020; Vazaios et al., 2018). Moosavi et al. (2018) used discrete element method (DEM) to evaluate the influence of microcracks with predefined intensities and orientations on the tensile fracture behaviours of rocks, focusing on the analysis of changes in the apparent Young's modulus, tensile strength, and fracture mode. Griffiths et al. (2017) analysed the influences of the aspect ratios of pores in elliptical hole and the angle between the direction of applied stress and the major axis of pores on the mechanical behaviours of porous rock under uniaxial compression using RFPA program. Bahrani and Kaiser (2016) investigated sample size effect on the strengths of defective and intact rocks based on SRM model by integrating a particle flow code (PFC) with DFN representing defect geometries. An SRM model coupling DFN and universal distinct element code (UDEC) was employed to characterise the scale-dependences of the mechanical and geometric characteristics of jointed rock masses (Farahmand et al., 2018).

As the solid part of rock mass, a rock block may contain defects with different structural characteristics, e.g. microcracks, holes and cemented joints, as shown in Fig. 1, all of which may affect its mechanical properties under different loading conditions. On one hand, due to the inherent variability, it is difficult to use data obtained from tests on natural rock samples to reveal the influences of specific parameters. On the other hand, conventional scale-effect analysis mainly focuses on the macro-discontinuity structures at a normal engineering-scale, ignoring the mesoscale and submacroscale, while the discontinuities at different scales vary. In addition, the existing literature mainly focuses on microcracks and voids, however, until now, few studies have been conducted on basalt with amygdale defects.

Hence, aiming at rock blocks at laboratory scale, amygdaloidal basalt sampled from the Baihetan Hydropower Station was taken as the research object in this study. An SRM model based on a combination of DFN and finite-discrete element method (FDEM) was presented to characterise the rock, and the influences of amygdale heterogeneity and sample size on the equivalent mechanical characteristics of basalt were explored. First, the distribution characteristics of the major axis length, orientation, and minor axis-major axis ratio of amygdales were statistically analysed, which were used to establish DFN models. Then, they were embedded into the FDEM numerical software to create SRM models. On this basis, a series of numerical tests under uniaxial compression was conducted to analyse the influences of amygdale heterogeneity (specific geometric parameters) on the mechanical properties of rocks separately, and to explore the size-dependences of geometric and mechanical properties of SRM models.

2. Structural characteristics of amygdaloidal basalt

Baihetan Hydropower Station, which is the largest hydropower plant being constructed globally, is located on Jinsha River lower reaches between Yunnan and Sichuan Provinces in southwest China (Fig. 2a). Geologically, the engineering site is located in the basalt formation of Emeishan with main lithologies of cryptocrystalline and amygdaloidal basalt. Besides geological structures with large scales, including dislocation zones, faults, joints, and cracks, which are exposed in basaltic rock mass, amygdaloidal structures at a mesoscale are common in the basalt (Zhang et al., 2013; Dai et al., 2016; Xia et al., 2019).

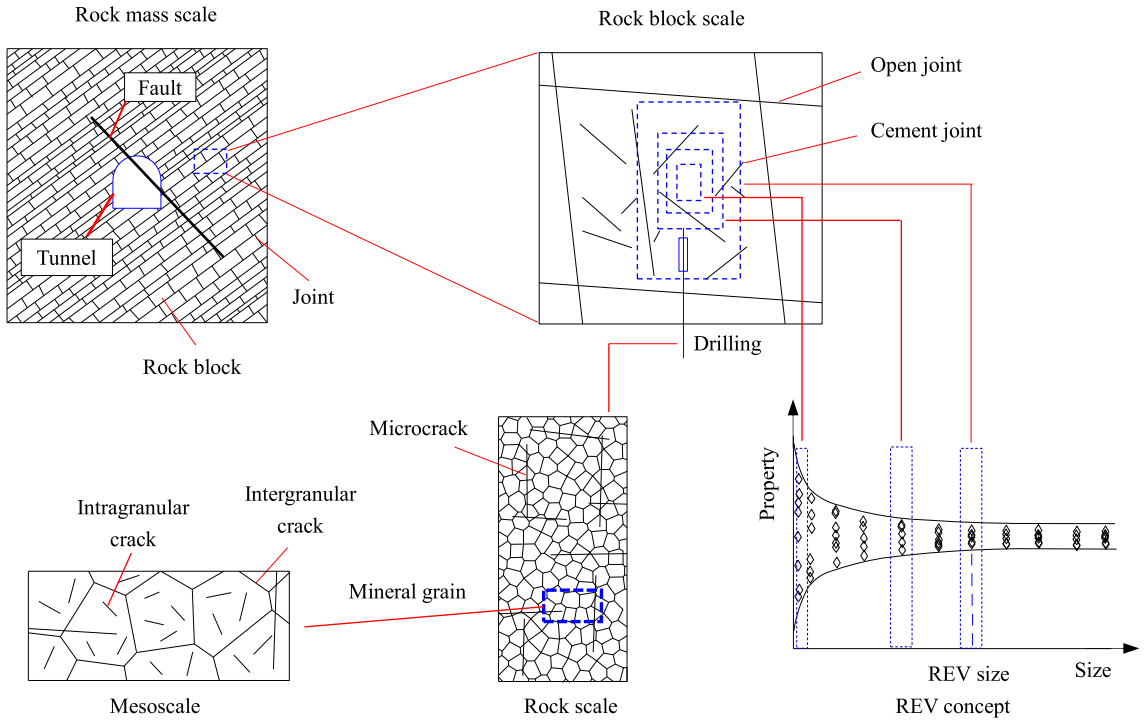

Fig. 1. Discontinuities at different scales in the rock mass and scale-dependence of rock mass properties. REV is the representative element volume.

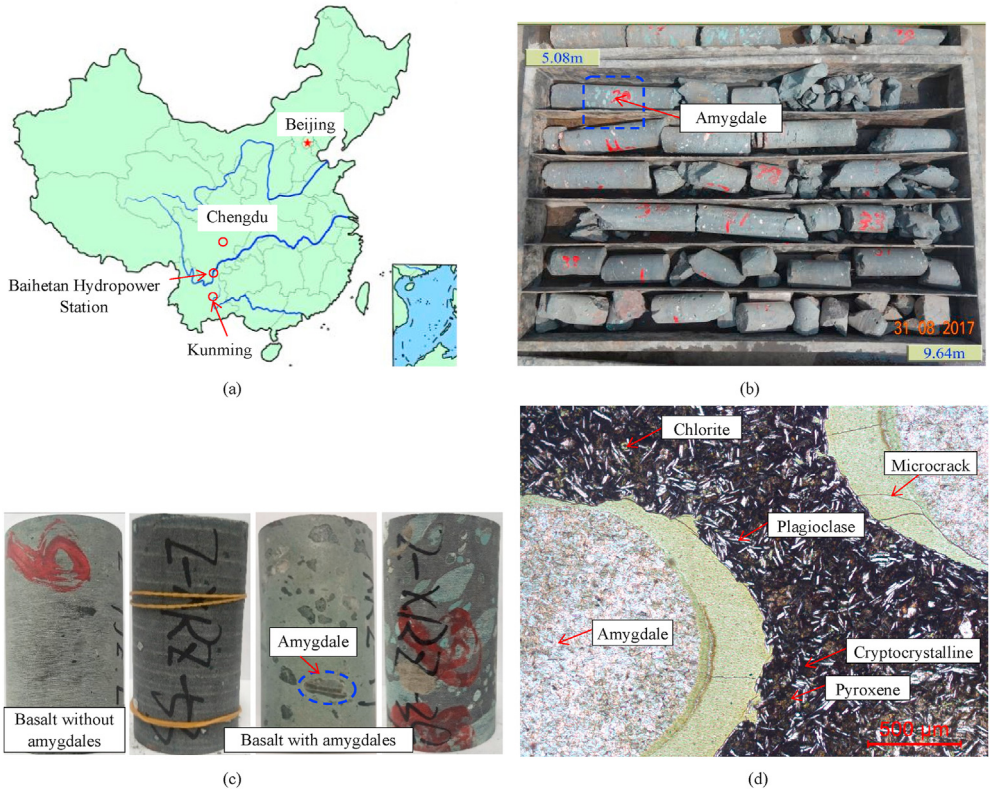

Fig. 2. Physical morphologies and microscopic structures of amygdaloidal basalt at Baihetan hydropower station: (a) Location of rock material, (b) Drilling cores from underground powerhouse caverns, (c) Basalt samples with varied geometric parameters of amygdales, and (d) A microscopic image of a thin section of amygdaloidal basalt.

As a kind of volcanic extrusive rock, basalt is a typical heterogeneous and usually contains heterogeneity in the form of holes and amygdales with varying size, shape, and abundance. The rock is cyan grey, dense and hard (Fig. 2b). Vesicular textures are volcanic rock textures in which rocks are pitted with several cavities (known as vesicles) that form on the surface of the Earth in a phenomenon called extrusion. Amygdale is another related texture, where secondary minerals such as calcite, quartz, and chlorite fill vesicles. The complexity during the diagenesis process of basalt leads to great variability in the geometric parameters of amygdales, for instance, the content of amygdales in rocks may be in the range of about 0 to about 1, the size spans several orders of magnitude (generally from a few tens of microns to millimetres or even centimetres), and shape can vary from slender to spherical, as shown in Fig. 2c. This huge heterogeneous structure is bound to exert an important effect on the failure mechanisms and physico-mechanical characteristics of rock (Baud et al., 2014; Heap et al., 2016).

2.1. Meso-structural characteristics of amygdaloidal basalt

Fig. 2d shows the orthogonal polarisation of amygdaloidal basalt. One can observe that there are many amygdales scattered thereon, accounting for about 20%–25% of the rock, and they are generally round and elliptical, with a characteristic size of 0.6–4 mm. They are mainly composed of chlorite mineral, with local quartz fillings. Matrix mineral composition mainly includes labradorite, cryptocrystalline, pyroxene, and a trace amount of chlorite. Labradorite is self-shaped lath with a major axis diameter range of 0.02–0.3 mm, and pyroxene is fine granular with a particle size range of 0.01–0.04 mm. Moreover, black vitreous material is a cryptocrystalline aggregate left uncrystallized during lava eruption.

In order to understand the physical properties of basalt, the density and longitudinal wave velocity of amygdaloidal basalt and cryptocrystalline basalt (without amygdales) for better comparison were tested, as shown in Fig. 3. It can be seen that the density of amygdaloidal basalt is basically in the range of 2650–3000 kg/m^3, with an average value of about 2800 kg/m^3, and the longitudinal wave velocity is mainly in the range of 3000–5000 m/s, with an average value of about 3900 m/s. The density of cryptocrystalline basalt is basically at 2750–3000 kg/m^3, with a mean value of about 2900 kg/m^3, and the wave velocity is basically at 4000–5000 m/s, with a mean value of about 4500 m/s. Compared with cryptocrystalline basalt, amygdaloidal basalt has a larger density and wave velocity distribution range, and the density and wave velocity values are significantly reduced, which reflects the defect structures in rock, showing a poor uniformity. It can be seen that amygdale structures with strong randomness and large dispersion inside basalt significantly affects its physical properties. The inhomogeneity of rock itself is bound to impose an important impact on its mechanical properties, leading to the discreteness and volatility of test results. To a certain extent, this increases the difficulty of testing and analysis. Therefore, it is necessary to conduct numerical analysis.

2.2. Statistics pertaining to amygdales

To construct the DFN model of amygdaloidal basalt (similar to DFN), the statistical analyses of the specific geometric parameters, such as density, orientation, and size of amygdales, were described to obtain the corresponding probability distribution models. This information can be used as the input parameters for generating DFN models (Lei et al., 2017). Since computed tomography (CT) scanning is expensive and the geometric analysis of amygdale

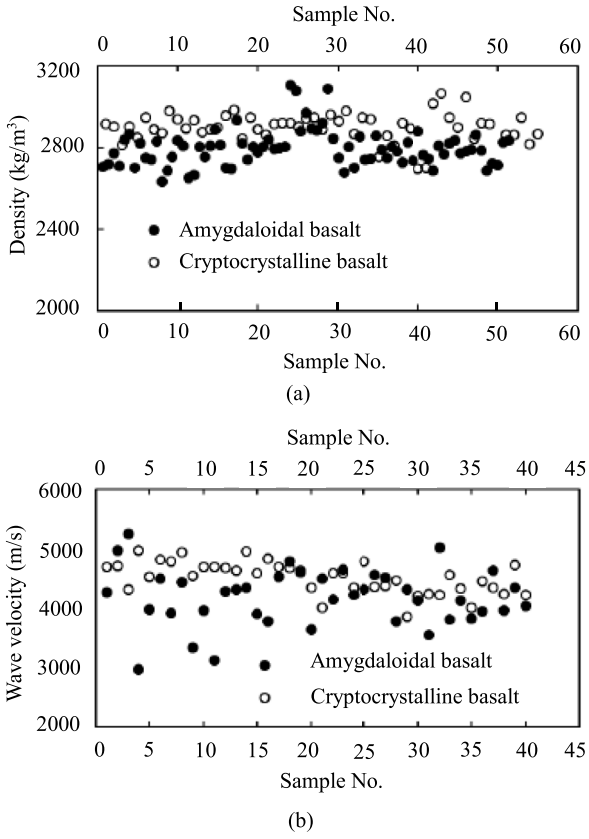

Fig. 3. Test results of (a) density and (b) sound wave velocity of basalt at Baihetan hydropower station.

morphology is difficult, scanning of the interior of sufficient amygdaloidal basalt samples is impossible; hence, measurement of amygdale statistics and geometric parameters was performed on only the surface of a large number of standard cylindrical samples, and the two-dimensional (2D) distribution characteristics were used to describe the three-dimensional spatial characteristics in the interior of the rock. Since most of the amygdales are approximately elliptical in two dimensions, they were simplified as equivalent ellipses. The geometric parameters obtained mainly include major axis orientation θ (considered as the angle between vertical axis and major axis), major axis length l, and the length ratio of minor to major axes of ellipse α.

According to the statistics pertaining to 2500 amygdales with a major axis length $\geq$1 mm in 18 cylindrical samples (Zhang et al., 2020), the corresponding statistical results of geometric parameters are as follows: θ conforms to a uniform distribution, and l exhibits a negative exponential distribution ($\lambda = 0.25$, correlation coefficient = 0.96), where λ is a parameter of the negative exponential distribution, which is often called the rate parameter. α conforms to a normal distribution ($\mu = 0.63$, $\sigma = 0.17$, correlation coefficient = 0.98), where μ is the mathematical expectation of the normal distribution and σ represents the standard deviation. Moreover, after calculation, the areal density P_{20} is 1.12 per cm^2, and the amygdale content (areal density P_{21}) is 14.66% (areal density P_{20} is defined as total amygdale number per sample unit area, and areal density P_{21} is total amygdale area per sample unit area).

3. Generation of the SRM model of amygdaloidal basalt

This section introduces the generation of the SRM model of amygdaloidal basalt combining a DFN model and an FDEM model, and the calibration process of corresponding meso-parameters. Although the actual basalt and amygdale structures are three dimensional, considering the limitations of computational capacity and time, they are treated as 2D scales.

3.1. Fundamental principles of FDEM

Combined FDEM is a numerical approach wherein a continuum mechanics principle (finite element method (FEM)) is combined with a discontinuous mechanics algorithm (DEM) for the simulation of several interacting deformable solid materials (Munjiza, 2004; Mahabadi et al., 2010; Lisjak and Grasselli, 2014; Yan et al., 2018). The modelling domain of FDEM is classified using a mesh comprising 3-node triangular finite elements and 4-node cohesive crack elements embedded coincident with all adjacent triangle pair edges. Elastic deformation of intact material is modelled based on linear elasticity continuum theory by employing constant-strain triangular finite elements. The calculation of contact forces is performed among all element pairs overlapping in space. Repulsive forces along normal direction among elements in contact with each other are determined according to a distributed contact force penalty function, whereas frictional forces among contacting couples are determined by a Coulomb-type friction law.

On the basis of the displacements of relative crack wall and local stress as well as Mohr–Coulomb and maximum tensile stress failure criteria, crack elements applied for the simulation of material progressive failures could experience mode I (tensile failure), mode II (shear failure), or mixed-mode I–II (tensile–shear failure) fracturing and yielding. Because multiple mechanical models and criteria for the initiation, propagation and coalescence of cracks are taken into account in the current approach, with no prior assumptions for the modes and paths of failure, cracks can freely expand within divided grids on the basis of the state of deformation and stress, including deformation, rotation, interaction, fracture, and fragmentation. Hence, the model could take into account progressive failure processes of brittle geo-materials from continuous to intermittent and finally discontinuous.

3.2. SRM model of amygdaloidal basalt

For amygdaloidal basalt, after determining the probability distribution forms and characteristic parameters of the geometric parameters of amygdales, a DFN model of amygdales could be established, and then a hybrid DFN-FDEM model representing amygdaloidal basalt can be established, which truly and accurately reflects the meso-structural characteristics of this rock. The corresponding generation steps are described as follows:

(1) Study area dimension was first determined, and corresponding ellipse number was calculated on the basis of the amygdale density. Taking the model measuring 50 mm × 100 mm (width × height) as an example, the number of ellipses is 56.
(2) According to the above statistical results of the geometric parameters of amygdales, the corresponding random variables were generated by Monte Carlo method, and the endpoint coordinates of major axis and minor axis of ellipses were calculated to generate a set of random ellipses.
(3) There was no overlapping among ellipses and ellipse-model boundaries, otherwise, new coordinates of centroid were assumed until all ellipses met the requirements. It should be noted that the random ellipse generated in this study is not a real DFN. Therefore, a similar DFN model is used, whose generation method and program are basically consistent with DFN model.

(4) The generated DFN model of amygdales was embedded into an FDEM code Irazu representing the complete matrix to construct an SRM model (DFN-FDEM) representing amygdaloidal basalt, which can consider the material heterogeneity at a mesoscale of the rock. The mechanical behaviours of the SRM model are controlled by the mechanical behaviours of rock matrix and amygdales.

The dimensions of the numerical samples of amygdaloidal basalt for calibration of meso-parameters were 50 mm × 100 mm (width × height), with the side length of the triangular elements being 1 mm, and two plates of loading were set on lower and upper ends (Fig. 4). A vertical displacement rate of 0.05 m/s with equal magnitudes along opposite directions at lower and upper ends was applied to achieving the axial loading (Abdelaziz et al., 2018). Various confining stress values corresponding to laboratory experiments were employed at the right and left boundaries of model and a plane strain model with 5×10^{-7} ms time step was adopted. Axial strain and stress were obtained through monitoring and calculating nodal displacements and forces on lower and upper loading plates, while lateral strains were determined based on monitoring and calculating node displacements at the middles of two sample sides, with approximately 10 mm width, in the same way to the measurement chain of hoop strain in the laboratory tests conducted using MTS equipment.

3.3. Calibration of meso-parameters in SRM model and numerical results

The meso-parameters used in FDEM model are classified as elastic parameters of triangular element (Poisson's ratio ν, elastic modulus E, and bulk density ρ), strength parameters of crack element (fracture energy G_f, internal friction angle φ, cohesion c, and tensile strength σ_t), and penalty values (P_n, P_t and P_f). Typically, fracture energy G_{f1} of tensile cracks is determined based on fracture toughness K_{Ic} estimated based on tensile strength derived from Brazilian disc splitting tests or obtained through three-point bending tests, and fracture energy G_{f2} of shear cracks is approximately $10G_{f1}$. The penalty values (P_n, P_t and P_f) are usually set at 10–100 times higher than elastic moduli. The model comprises two materials (amygdales and matrix), wherein the values of parameters for matrix are determined by referring to cryptocrystalline basalt (pure matrix) test results and they are reduced appropriately to give amygdale parameter values as the main component of amygdales is weaker chlorite (Liu et al., 2019). The interface between amygdale and matrix is simulated by a cohesive crack model. The calibration procedure used in the present work is an iterative process (a trial-and-error approach) which is performed through a series of numerical tests (uniaxial compression, biaxial compression and Brazilian disc splitting) to determine multiple meso-parameter values (Table 1), so that the macro-mechanical parameters of numerical simulation match the test results (Wang and Cai, 2019).

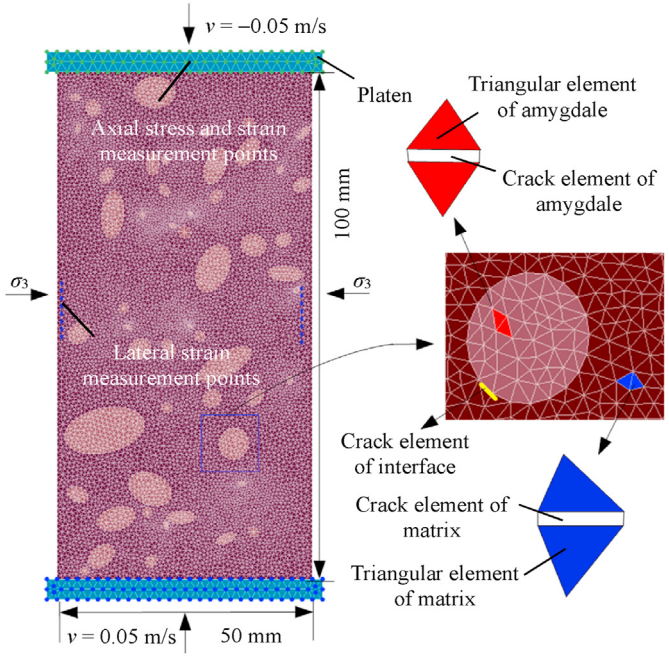

Fig. 4. An SRM model of amygdaloidal basalt for calibration of meso-parameters.

Fig. 5 shows the typical deviatoric stress–strain curves for amygdaloidal basalt samples exposed to various confining stress levels from numerical simulations and laboratory tests, in which the solid line represents the numerical results, and the dotted line represents the test results. It can be seen from the dotted line that under low confining stresses, the concave-up trend of the curve during the initial compaction stage is more obvious, which reflects the compaction response of a sample containing many initial defects (such as amygdales) in rock. Under increasing loading, the pre-peak curve is linear and the post-peak stress drops rapidly, showing a significant brittleness. As the confining stress increases, the initial compaction stage of the curve almost disappears. The pre-peak curve is quasi-linear, and the ductile yield plateau and zig-zag pattern are developed close to peak stress, with the range of stress fluctuations becoming increasingly wide. In addition, the post-peak stress decreases slowly, showing a transition from brittleness to ductility, which is similar to the brittleness-ductility transformation characteristics exposed under medium and high confining stress values for other hard brittle rock types such as marble (Liu et al., 2012; Zong et al., 2016).

It can be seen from the solid line that the initial compaction stage of curve of numerical samples is not obvious, and the mechanical behaviours of pre-peak curve show linear characteristics. The curve near the peak is zig-zag shaped, with the stress continuing to rise after a small drop, and the post-peak stress decreases. With the increase of confining stress, curve fluctuation range around the peak is increased progressively, yield platform appears, and post-peak stress is decreased slowly, gradually transforming from brittle to ductile behaviour. In summary, the stress-strain curves drawn by laboratory tests and numerical simulations are consistent.

According to Table 2, the macro-mechanical parameters of samples derived from numerical simulations agree with laboratory

Table 1
Meso-parameters of amygdaloidal basalt in FDEM (Zhang et al., 2020).

Meso-parameter	Value		
	Matrix	Amygdale	Interface
Bulk density, ρ (kg/m^3)	2900	2000	
Poisson's ratio, ν	0.15	0.2	
Young's modulus, E (GPa)	45	15	
Internal friction angle, φ(°)	39	30	35
Cohesion, c (MPa)	65	16	30
Tensile strength, σ_t (MPa)	18.5	4	8
Mode-I fracture energy, G_{f1} (N/m)	100	30	50
Mode-II fracture energy, G_{f2} (N/m)	1000	300	500
Normal contact penalty, P_n (GPa m)	450	150	300
Tangential contact penalty, P_t (GPa/m)	450	150	300
Fracture penalty, P_f (GPa)	450	150	300

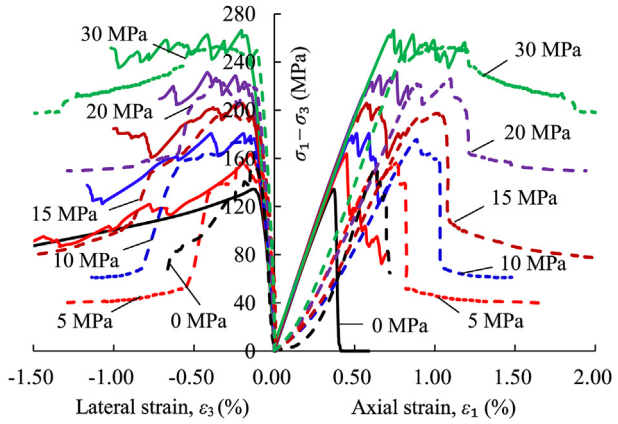

Fig. 5. Deviatoric stress-strain curves of amygdaloidal basalt samples (Zhang et al., 2020).

Table 2
Macro-mechanical parameters of amygdaloidal basalt from laboratory test and numerical simulation (Zhang et al., 2020).

Case	E (GPa)	ν	c (MPa)	φ (°)	σ_c (MPa)	σ_t (MPa)	σ_{ci}/σ_c	σ_{cd}/σ_c
Laboratory test	36.3	0.18	32.02	42.8	130.44	9.6	0.45	0.9
Numerical simulation	36.56	0.19	30.52	42.9	134.4	10.1	0.47	0.92

Table 3
Numerical simulation scheme of influence of geometric parameters of amygdales on strength. "↑" indicates that a certain parameter changes, and "-" indicates that a certain parameter remains unchanged.

Variable	m	l	α	θ
m	↑	–	–	–
l	–	↑	–	–
α	–	–	↑	–
θ	–	–	–	↑

test results, indicating that numerical model and the selected meso-parameters used in the present research are reliable, based on which the numerical results can depict the main mechanical behaviours of amygdaloidal basalt.

4. Effect of amygdale heterogeneity on mechanical characteristics of basalt

In this section, a series of numerical tests was performed based on the created SRM model of basalt to explore the influence of this structural heterogeneity on the equivalent mechanical characteristics of rock from the quantitative point of view, focusing on the analysis of the influences of specific geometric parameters, such as the number m, size l, orientation θ (angle between major axis direction and loading direction or vertical direction) and aspect ratio α of amygdales.

4.1. Numerical simulation scheme

Table 3 lists the numerical simulation algorithm on the basis of geometric factor changes. For the four geometric variables m, l, α and θ, when one of them changes, other three variables remain unchanged. The typical geometric models generated by the change of each variable are shown in Fig. 6, wherein the geometric dimensions are the same as those shown in Fig. 4. In addition, the numerical samples were obtained on the basis of statistical findings presented in Section 2.2. Due to a high time-cost of numerical calculation in FDEM, it is impossible to conduct the calculation for many samples. In addition, to ensure the statistical reliability of the calculation results, 20 realisations were generated for each numerical test scheme in the present study.

For each sample, the numerical simulation of uniaxial compression test was carried out, whose boundary conditions and meso-parameters used are consistent with those in the calibration model (standard sample). Based on the numerical results, the influence of the heterogeneity of amygdale structure on the equivalent mechanical properties of rock was quantified.

4.2. Numerical results and analysis

Peak stress σ_f, crack damage stress σ_{cd}, and crack initiation stress σ_{ci} are characteristic stress thresholds between several important stages representing the progressive failure process of brittle rock. They are of significance in the understanding of the progressive fracture process of rock and failure mechanism and predicting failure range and long-term stability of surrounding rock mass in underground engineering operations conducted under high-stress conditions. In laboratory tests on intact rock, σ_{ci} is described as the stress threshold of stable crack growth, corresponding to the occurrence of micro-fractures, which is approximately 40%–60% of σ_f. σ_{cd} is assumed to be the stress of the appearance of unstable cracks, which corresponds to coalescence and penetration of a large number of microcracks, at around 70%–85% of σ_f. σ_f is widely applied for establishing the envelope curves of rock strength. There are several methods used to determine these characteristic stresses. These characteristic stresses (σ_{ci}, σ_{cd} and σ_f) of amygdaloidal basalt are estimated from the analyses of crack volume-strain curve, total volume-strain curve, and stress-strain curve of the numerical samples in this research, combined with the trend in evolution of microcrack number and lateral strain difference method (LSR), in which σ_{ci}/σ_f and σ_{cd}/σ_f are characteristic strength ratios (for details of these methods, please refer to Martin and Chandler (1994), Cai et al. (2004), Hoek and Martin (2014), and Zhao et al. (2015)).

4.2.1. Effect of the quantity of amygdales

To investigate the influence of amygdale number on the equivalent mechanical characteristics of basalt, the number of amygdales m in the numerical samples is set to 14, 28, 56, 84, 112 and 168, a total of six working conditions, where $m = 56$ is the average value of the number of amygdales. The relationship between the mechanical properties of basalt by numerical simulation and the number of amygdales obtained is shown in Fig. 7, where the scattered points represent the values of mechanical properties in different samples calculated under the same working condition, and the broken line points denote the average values of the corresponding properties of all samples calculated under the same working condition (as below).

The Young's modulus E decreases linearly from 43.59 GPa to 26.5 GPa with the increase in number of amygdales m, a reduction of 40%. The UCS (peak strength σ_c) shows logarithmic decay, decreasing from 350 MPa to 84.04 MPa, a reduction of 76%. Meanwhile, the decreasing trend is most obvious when m is small and tends to be stable as m increases. The trends in σ_{ci}, σ_{cd} and σ_{cd}/σ_c are similar to that of σ_c, while σ_{ci}/σ_c tends to decrease significantly at first and then increases slightly. In addition, with the increase in m, the overall discreteness of the calculated results decreases. In other words, as the number of amygdales increases,

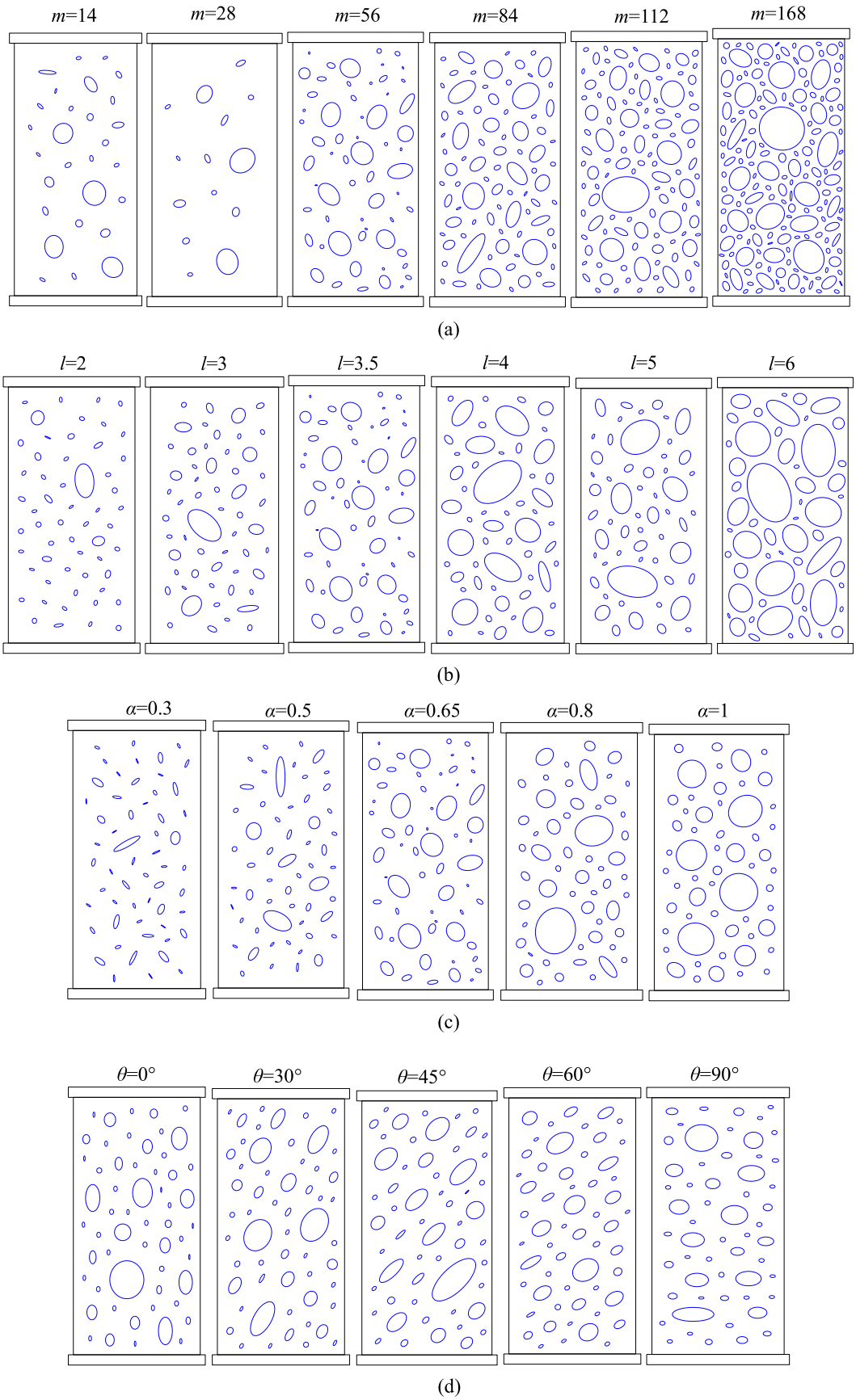

Fig. 6. DFN models of amygdaloidal basalt with varied geometric parameters for uniaxial compression tests: (a) Number of amygdales (m), (b) Size of amygdales (l), (c) Aspect ratio of amygdales (α), and (d) Orientation of amygdales (θ). Twenty realisations were generated for each set of geometric parameter conditions.

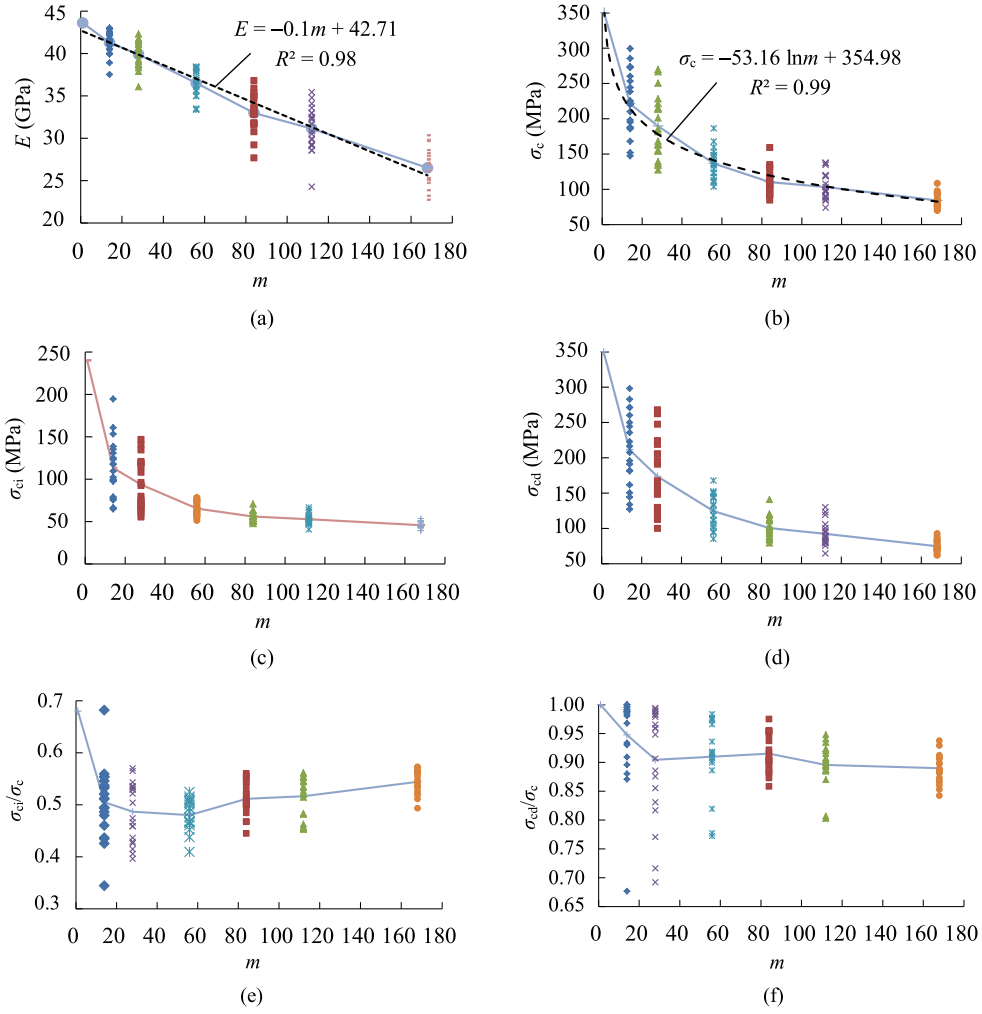

Fig. 7. Influence of number of amygdales on the mechanical properties of basalt: (a) E, (b) σ_c, (c) σ_{ci}, (d) σ_{cd}, (e) σ_{ci}/σ_c, and (f) σ_{cd}/σ_c.

the overall area occupied by them also increases, and the macro-mechanical properties of samples tend to be uniform.

The relationships of E and σ_c with m obtained through least-squares fitting are as follows:

$$\left.\begin{array}{ll} E = -0.1m + 42.71 & (m \geq 1) \\ \sigma_c = -53.16\ln m + 354.98 & (m \geq 1) \end{array}\right\} \quad (1)$$

4.2.2. Effect of the size of amygdales

To investigate the influence of amygdale size on the equivalent mechanical properties of basalt, the major axis length of amygdales l is taken as 2 mm, 3 mm, 3.5 mm, 4 mm, 5 mm and 6 mm. This gave a total of six working conditions, among which $l = 3.5$ mm is the mean value of the major axis length of amygdales. The relationship between the mechanical properties of basalt as derived from numerical simulations and l is presented in Fig. 8, in which the changes in E and σ_c is close to those shown in Fig. 7.

As l increased, the change in E is similar to that when the parameter m is changed, and the change is linear. The UCS (peak strength σ_c) decreases from 350 MPa to 75.81 MPa with the increase in l, which decreases by 78% in an exponential manner. Meanwhile, the reduction rate of σ_c is larger when l is smaller. The σ_{ci}, σ_{cd} and σ_{cd}/σ_c are consistent with the trend in σ_c, while the σ_{ci}/σ_c first decreases and then increases. In addition, as l increases, the global discreteness of the calculated results also decreases significantly.

Through least-squares fitting, the relationships of E and σ_c with l are as follows:

$$\left.\begin{array}{l} E = -2.83l + 45.56 \\ \sigma_c = 350.8e^{-0.26l} \end{array}\right\} \quad (2)$$

4.2.3. Effect of the aspect ratio of amygdales

To better comprehend the effect of amygdale aspect ratio on the mechanical characteristics of basalt, minor-major axes ratio α is set to 0.3, 0.5, 0.65, 0.8 and 1 giving five operating conditions, where $\alpha = 0.65$ is the mean value of the aspect ratio of amygdales. The relationship between the macro-mechanical properties of basalt derived from numerical simulations and α is presented in Fig. 9, where the changes in E and σ_c is close to those shown in Figs. 7 and 8.

With the increase in α, E decreases linearly from 43.59 GPa to 32.97 GPa, with a reduction of 25%, and the UCS (peak strength σ_c) undergoes logarithmic decay, decreasing from 350 MPa to 110.1 MPa, with a reduction of 70%. The trends in σ_{ci}, σ_{cd} and σ_{cd}/σ_c are similar to that of σ_c, while σ_{ci}/σ_c decreases significantly at first and then increases slowly.

The relationships of E and σ_c with α obtained through least-squares fitting are as follows:

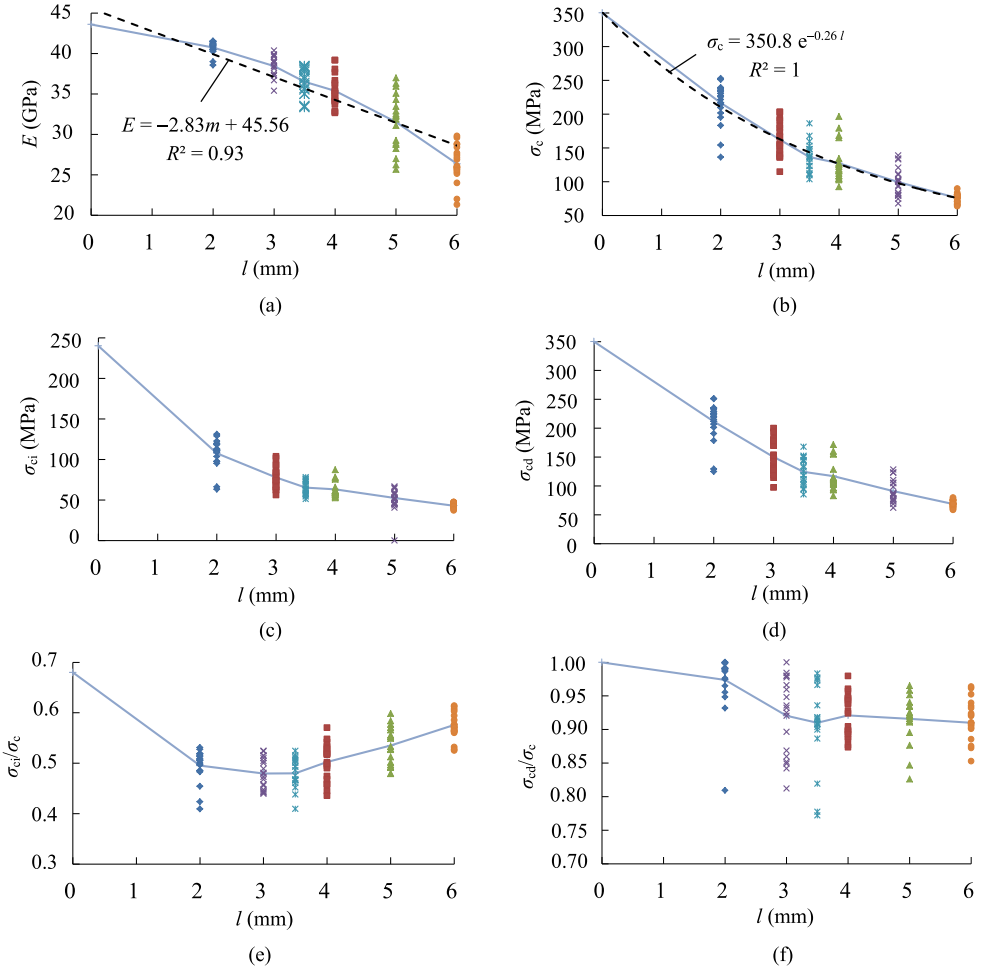

Fig. 8. Influence of amygdale size on the mechanical properties of basalt: (a) E, (b) σ_c, (c) σ_{ci}, (d) σ_{cd}, (e) σ_{ci}/σ_c, and (f) σ_{cd}/σ_c.

$$\left.\begin{aligned} E &= -10.52\alpha + 43.18 \quad (0 < \alpha \le 1) \\ \sigma_c &= -52.22\ln\alpha + 110.29 \quad (0 < \alpha \le 1) \end{aligned}\right\} \tag{3}$$

4.2.4. Effect of the orientation of amygdales

The mechanical behaviour of rock with defects is largely controlled by the spatial distribution characteristics of the defects, especially when these defects are oriented in a certain direction. The macro-mechanical response of rock often shows anisotropic characteristics. To grasp the influence of orientation arrangement of amygdales on the macro-mechanical properties, the orientation θ is taken as 0° (parallel to the loading direction), 15°, 30°, 45°, 60°, 75° and 90° (perpendicular to the applied loading), giving a total of seven working conditions. The relationship between the macro-mechanical properties of samples obtained by numerical simulation and θ is presented in Fig. 10.

It is observed that with the increase in orientation θ of amygdales in the range of 0°–90°, the change trend in the macro-mechanical properties is not obvious. The Young's modulus E decreases slowly from 36.81 GPa to 35.4 GPa, i.e. E is the largest when the amygdales lay parallel to the loading direction. The UCS (peak strength σ_c), σ_{ci} and σ_{cd} decrease slightly at first and then increase, all of which are the lowest when $\theta = 60°$. The trends in σ_{ci}/σ_c and σ_{cd}/σ_c run contrary to those of σ_{ci} and σ_{cd}, which first increase and then decrease, i.e. the characteristic strength ratios are minimised when the dip angle is 90° (parallel to the loading direction). Therefore, amygdaloidal basalt exhibits relatively significant strength and stiffness anisotropy.

5. Scale-dependences of geometrical and mechanical properties of amygdaloidal basalt

5.1. Numerical simulation scheme

Firstly, a 2D DFN model with sufficiently large size (2000 mm × 2000 mm) was generated based on the statistical data of distribution characteristics for the amygdales. Then, random sampling was performed within its range to generate multiple DFN models of smaller sizes, whose width d is 25 mm, 50 mm, 75 mm, 100 mm, 150 mm, 200 mm, 300 mm, 400 mm and 500 mm, respectively, with a constant aspect ratio of 2, as shown in Fig. 11. Based on the measured amygdale content (areal density P_{21}), the size-dependence of the geometric parameters of amygdaloidal basalt blocks was analysed to obtain the corresponding REV. On this basis, some of the DFN models above were embedded into the FDEM to create corresponding SRM models of different sizes. According to the aforementioned boundary conditions and meso-parameters, a series of numerical tests under uniaxial compression was conducted on these SRM models to analyse the influence of sample size on the strength of amygdaloidal basalt blocks. Similarly, to eliminate this potential randomness and take into account the constraints of computing time, the SRM models were created 3–20 times at each scale; the larger the size, the smaller the number of modes.

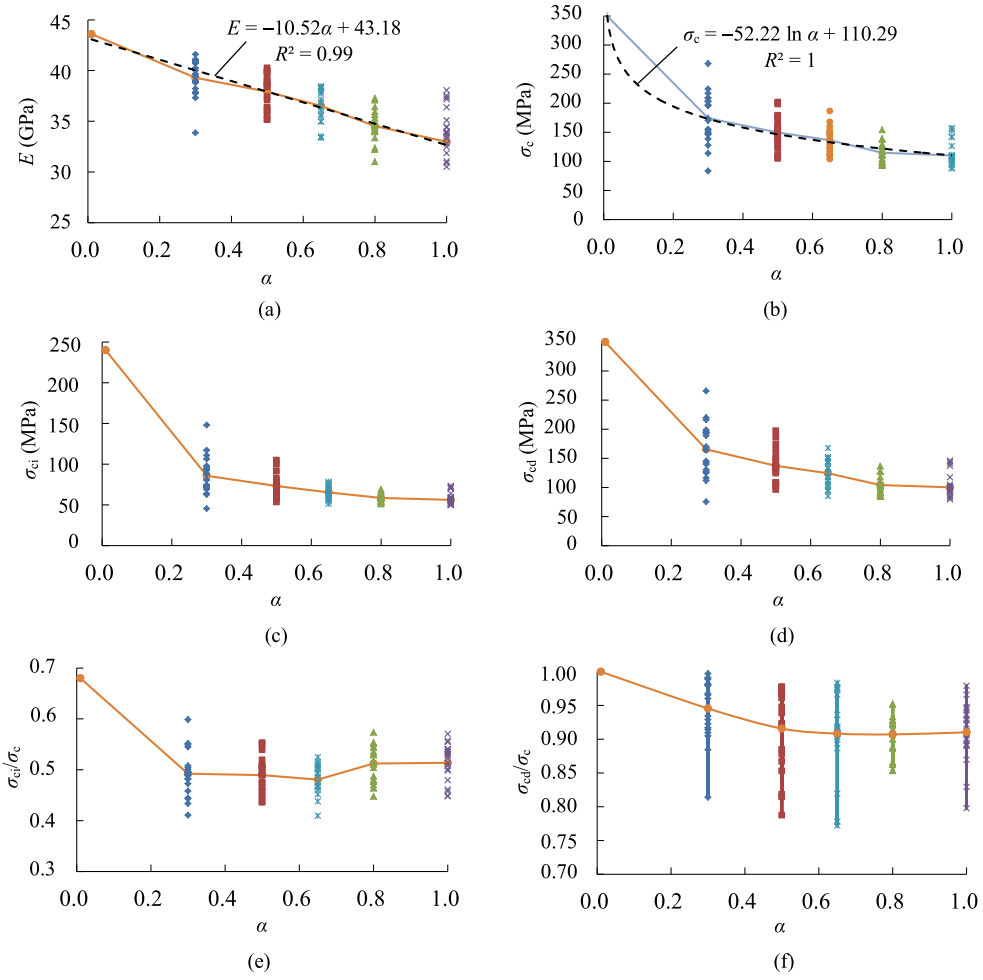

Fig. 9. Influence of aspect ratio of amygdales on the mechanical properties of basalt: (a) E, (b) σ_c, (c) σ_{ci}, (d) σ_{cd}, (e) σ_{ci}/σ_c, and (f) σ_{cd}/σ_c.

5.2. Numerical results and analysis

5.2.1. Size-dependence of geometrical parameters

To assess the influence of sample size on geometric properties of amygdaloidal basalt blocks, the amygdale content (areal density P_{21}) and its coefficient of variation (CoV) of multiple DFN models at different sizes were measured. The REV of geometric properties was determined based on the variation degree of P_{21}. As shown in Fig. 12, the scattered points represent discrete data of P_{21} of different samples (20 samples) at the same size, the blue line denotes the mean of these discrete data, and the orange line denotes its CoV which is described as standard deviation-average value ratio. Also, in this study, an acceptable CoV is less than 10% (Farahmand et al., 2018).

The average value of P_{21} of different samples at each size is unchanged (fluctuating slightly only at small sizes), at about 14.5%, which is consistent with the data obtained from the statistical characteristics of amygdales. This indicates that no matter how large the sample size, the defect content in the sample is similar, and it does not increase gradually with increasing size. With the increase in sample size, the CoV decreases nonlinearly, and the decrease trend is more pronounced at small sizes. For the samples with small sizes (smaller than 100 mm), the CoV is more than 20%, and P_{21} dispersion across different samples of the same size is obvious, indicating that the number of defects within the samples at these sizes cannot represent the structural characteristics of the overall rock block. When the sample sizes are 100–150 mm, the CoV decreases to 10%–15%, at which the fluctuation range of P_{21} becomes significantly narrower. However, for samples larger than 200 mm, the CoV is below 10%, and P_{21} tends to be stable, indicating that defect population in samples is high enough to represent the overall conditions of rock block. Hence, the geometric REV size of 200 mm was characterised on the basis of aforementioned parameter variabilities.

5.2.2. Size-dependency of the strength

In this section, the strength and CoV of multiple SRM models at different sizes were calculated, and the mechanical REV was obtained according to variability degree change of UCS (i.e. σ_c). As shown in Fig. 13a, as the sample size increases, the average value and CoV of σ_c of SRM models decrease, especially for smaller samples, and remain almost constant beyond a certain size. In addition, dispersion degree and fluctuation range of different samples of the same size decrease significantly. For sample smaller than 100 mm, the CoV is greater than 15%, and the fluctuation range of σ_c is notably wider, which indicates that a model with this dimension cannot be considered as statistically homogeneous due to the lack of the possibility of obtaining stable ranges of properties. When the sample sizes are 100–150 mm, the CoV decreases to about 10%, and the fluctuation range of σ_c at this size is narrower. For samples larger than 200 mm, the CoV is always below 10%, which is below acceptable value of CoV to establish REV size, and overall σ_c at this size tends to be asymptotic. Therefore, the mechanical REV size of 200 mm was characterised based on the

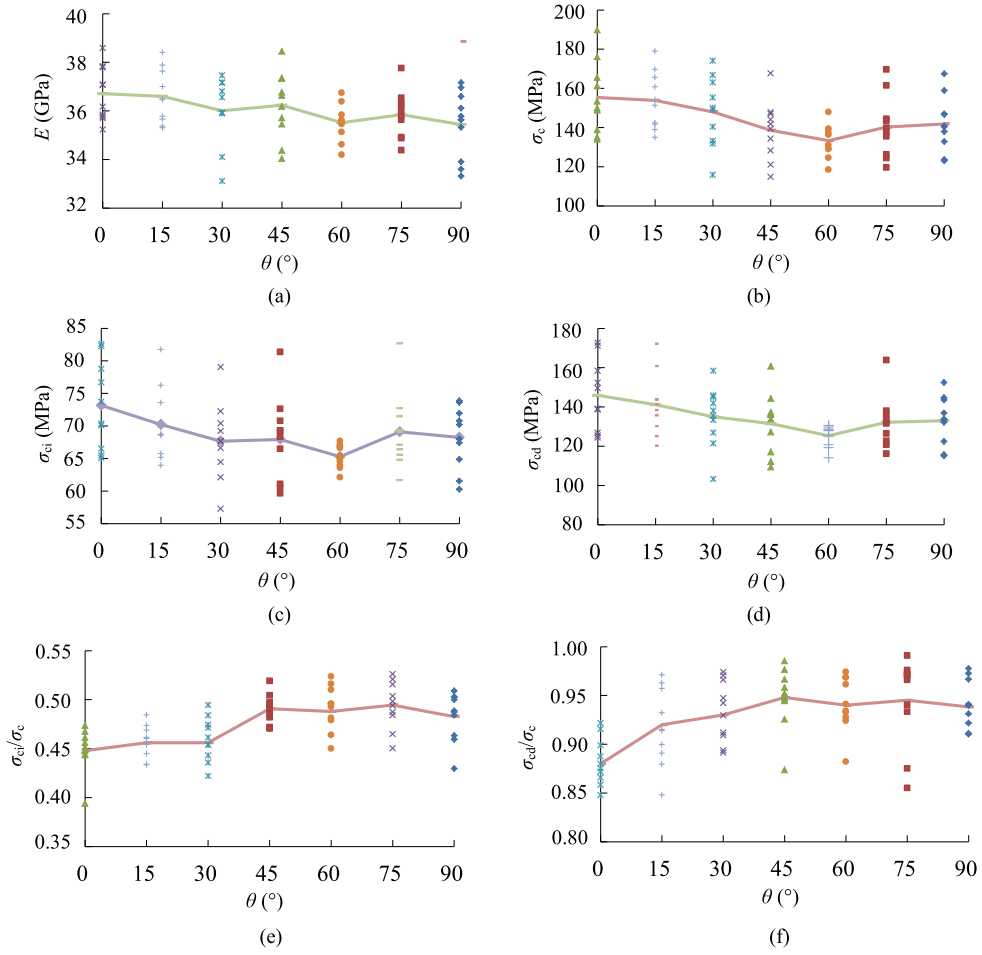

Fig. 10. Influence of orientation of amygdales on the mechanical properties of basalt: (a) E, (b) σ_c, (c) σ_{ci}, (d) σ_{cd}, (e) σ_{ci}/σ_c, and (f) σ_{cd}/σ_c.

dispersion degree and fluctuation range of the σ_c of samples with different sizes. The σ_c at the REV size is approximately 96.87 MPa, about 71% of that of the standard sample.

Similarly, with the increase in sample size, the dispersion and mean value of σ_{ci} and σ_{cd} for different samples with the same size exhibit a similar trend to that in σ_c. On the contrary, the average value of σ_{ci}/σ_c and σ_{cd}/σ_c for different samples with the same size keeps increasing with the size and tends to be stable. This shows that with the increase in sample size, the established SRM models are more uniform, and the characteristic strength ratios are continuously increasing, which can represent the entire rock mass and its condition.

In summary, an ultimate REV of 200 mm for amygdaloidal basalt blocks was determined according to the size-dependence of mechanical and geometric features. The mechanical features achieved at this scale are regarded as equivalent continuum properties and may be applied as the input parameters for larger-scale rock mass simulation based on a continuum approach.

6. Discussion

6.1. Effect of heterogeneity content on the strength

Based on the analysis in Section 4.2, the effects of the number, size and aspect ratio of amygdales on the mechanical properties of basalt are similar because they all affect the amygdale content (areal density P_{21}). Therefore, a relationship between the content of amygdales and rock strength was revealed and this result was compared with those from the literature. The interior of a rock mass contains defects with different structural features, such as microcracks, holes (filled holes) and amygdales, all of which may affect their mechanical behaviours. Fig. 14 shows the relationship between the defect content of different rock types and the UCS.

It can be seen from Fig. 14 that the best fitting curve of the relationship between simulated UCS (i.e. σ_c) and microcrack density in intact Lac du Bonnet (LdB) granite is an exponential decay function, in which with the increase in microcrack density from 0 to 0.2 mm/mm^2, σ_c decreases from about 190 MPa to 100 MPa (Hamdi et al., 2015). The relationship between σ_c of the volcanic rock containing circular holes with a diameter of 0.5 mm and porosity is quasi-exponential, in which σ_c decreases from 548 MPa at porosity of 0–47 MPa at porosity of 0.4, with a strength reduction factor of 0.91. For the volcanic rock containing circular crystals (filled holes) with a diameter of 1 mm, the σ_c and crystal fraction show a quasi-logarithmic relationship, in which the σ_c decreases from 458 MPa to 337 MPa by enhancing crystal fraction from 0.02 to 0.4, with a strength reduction factor of 0.38. Therefore, increasing porosity or crystal fraction decreases volcanic rock strength on which the effect of pore fraction is greater than that of crystal fraction (Heap et al., 2016). Similar to the volcanic rock with circular crystals, the best fitting curve between amygdale content and σ_c of basalt in this study shows a logarithmic relationship, in which the strength reduction of basalt is more significant at lower amygdale contents, and the strength tends to be stable at larger amygdale contents. With the increase in amygdale content from 0 to 0.44, the σ_c

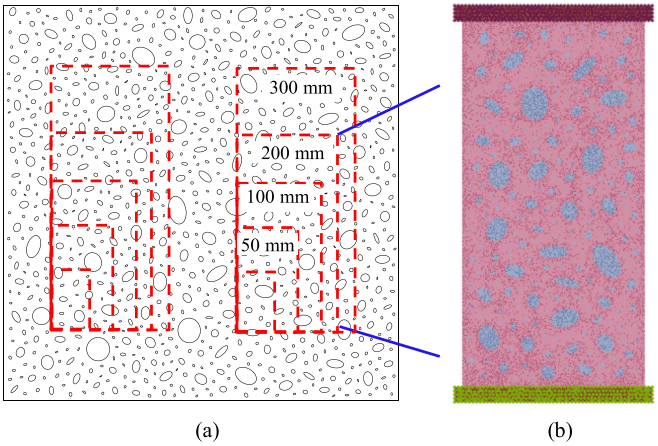

Fig. 11. SRM models of amygdaloidal basalt blocks with different sizes: (a) DFN models with different sizes, and (b) SRM model with size of 100 mm × 200 mm.

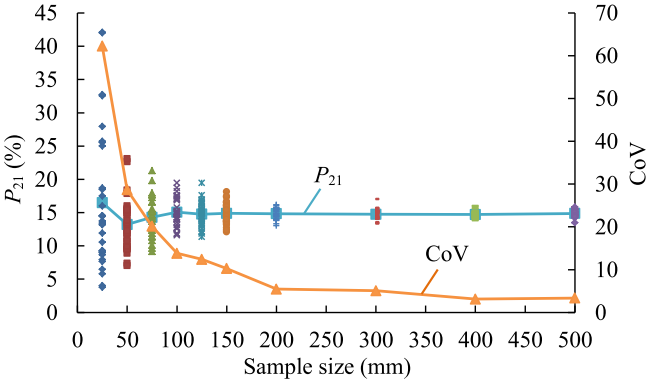

Fig. 12. Influence of sample size on P_{21}.

decreases from about 350 MPa to as low as 75.81 MPa, with a strength reduction factor of 0.78.

Therefore, defects play key roles in controlling rock strength, which decreases with increasing defect content; however, for different types of defects, such as microcracks, holes, crystals (filled holes), or amygdales, the change in strength caused by defect content differs. For defects, such as microcracks and holes, the strength decreases exponentially with increasing defects; however, when the defects are filled holes, such as crystals or amygdales, the strength decreases logarithmically with increasing defect content. In addition, the reduction in σ_c of rock with filled holes (including volcanic rock with crystals and amygdaloidal basalt) is smaller compared with that in porous volcanic rock.

6.2. Effect of heterogeneity angle on the strength

Various kinds of defect fabrics are found, such as bedding in sedimentary rocks, schistosity and gneissism in metamorphic rocks, and holes in volcanic rocks. These significantly affect the mechanical properties of the rocks. The results in this study were compared with the experimental or numerical data of strength anisotropy in the recent literature (Fig. 15). For sedimentary rocks and metamorphic rocks, the preferential orientation of defects on the horizontal axis is in accordance with the angle between schistosity or bedding and applied stress. For volcanic rocks with holes or amygdales, orientation is in accordance with the angle between major axis of amygdales or holes and applied stress. The normalised UCS (i.e. σ_c) on the longitudinal axis is expressed as $\sigma_{c\theta}/\sigma_{c0}$, a ratio representing the strength anisotropy, where σ_{c0} is defined as the σ_c at a defect orientation of 0°, and $\sigma_{c\theta}$ represents the σ_c or peak stress at other defect orientations.

For shale or gneiss, as this orientation of bedding or schistosity increases from 0° to 90°, the σ_c first decreases and then increases (with a maximum at 0° or 90° and minimum at about 45°) (Cho et al., 2012). For elliptical voids in infinite media, volcanic rocks or basalts with holes, the σ_c continues to decrease with the increase in the angle between applied stress and major axis of holes from 0° to 90, i.e. the sample strength is the highest when the major axis direction of holes is parallel to the loading direction, and it is the lowest when the major axis direction of holes is perpendicular to the loading direction. This is consistent with the analysis of the concentration of stress around one elliptical hole (Bubeck et al., 2017; Griffiths et al., 2017). Therefore, defective rocks containing bedding or elliptical pores with preferential orientation can exhibit considerable strength anisotropy. For amygdaloidal basalt, as the angle between loading direction and major axis of amygdales increases, the σ_c first decreases and then slightly increases (with a maximum at 0° and minimum at 60°). Its overall trend is slightly different from that of other rocks, and the decrease in strength is small, leading to lower strength anisotropy compared to other geologic media. This is because an amygdale is a result of pores being filled by other minerals under later geological action, which is not in complete consistency with the effects of simple bedding and pores.

Crustal rock strength anisotropy is usually assigned to the preferential alignment of the existing defect structures such as layer planes, holes or fillings inside. However, strength evolution for the angle between each of these fabric directions and applied stress is markedly different. Several mechanical anisotropy sources in crust along with their different contributions thereto indicate the significance of orienting rocks either catalogued or collected in field and provide a comprehensive description for their textural heterogeneity.

6.3. Influence of sample size on the strength

Generally, the effect of sample size refers to the effect of rock sample size with a constant ratio of slenderness, including the scale effect of different properties, such as geometry, mechanics, hydraulics and temperature. The most commonly applied size effect relation was introduced by Hoek and Brown (1980), who suggested a power function in normalised form to correlate the σ_c of intact rock samples with a certain diameter d to that of a sample with 50 mm in diameter, as presented in Fig. 16. The equation is expressed as $\sigma_{cd}/\sigma_{cd50} = (50/d)^{0.18}$, in which σ_{cd} and σ_{cd50} are the σ_c values of the samples with arbitrary and 50 mm diameter, respectively; and d is the sample diameter (mm). The normalised σ_c decreases with the increase in sample size, which is attributed to the enhanced heterogeneity of rock by volume and greater probability of micro-defects to allow unstable propagation of cracks. When the sample contain enough defects, a constant value of strength may appear corresponding to the REV, which is the smallest volume where the test results are independent of sample size and can represent the whole rock.

However, Hoek and Brown (1980)'s formula only represents rocks with good integrity and homogeneity and may overestimate the strength of samples with micro-defects or those affected by weathering or temperature (Stavroua and Murph, 2018). For the marble samples heated at the temperature of 200 °C, the variation trend of normalised σ_c with sample size agrees well with Hoek and Brown (1980)'s model. On the other hand, strength decrease after thermal damage with increasing sample size is intensified, thus

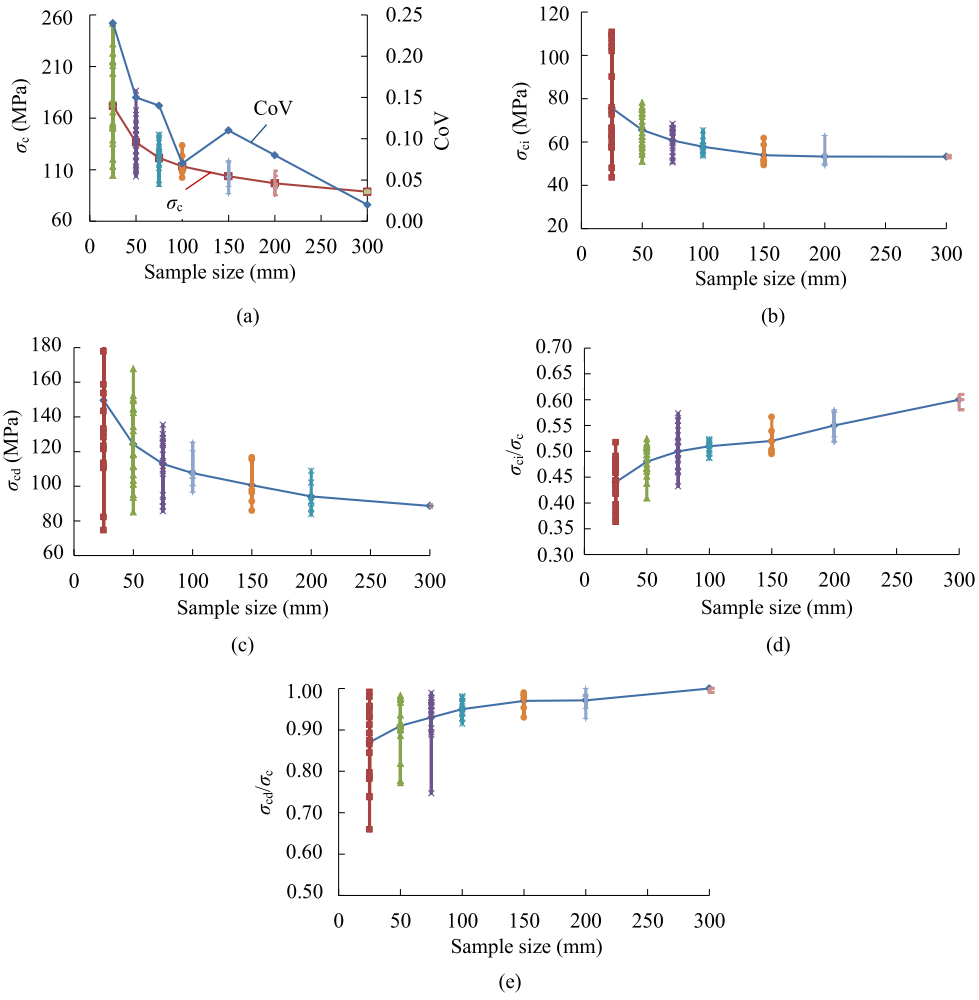

Fig. 13. Influence of SRM sample size on the strength: (a) σ_c, (b) σ_{ci}, (c) σ_{cd}, (d) σ_{ci}/σ_c, and (e) σ_{cd}/σ_c.

increasing model's exponent (Guan et al., 2018). For amygdaloidal basalt, due to the presence of more defects on a mesoscale, the size effect of strength is more severe. Therefore, there is no general law applicable to the size effect of rock strength, which has a close relation with lithology, heterogeneity type, and the structure and size of fractures.

The size effect of the strength of rock mass is a key bridge from which to establish the relationship between the mechanical properties of rock sample and in situ rock mass, which can provide an important basis for the estimation of mechanical features of rock masses based on the test results of mechanical properties of standard laboratory samples. When the sample size increases gradually from the standard sample size in the laboratory, the size and structure of the defects in the samples constantly change, and the mechanical properties of the samples change accordingly. For the same sample size, the distribution of defects in the samples is obtained by random sampling, thus the mechanical properties of samples exhibit natural variability. Therefore, the mechanical properties mentioned here refer to the average value of a certain quantity of samples. Of course, with the increase in sample size, the discreteness in the sampling process becomes smaller, and the defect density in the samples is unchanged regardless of sampling method. Therefore, the discreteness of their mechanical properties also decreases accordingly.

7. Conclusions

In this study, aiming at the rock blocks of amygdaloidal basalt at the laboratory scale, an SRM model based on the combination of DFN and FDEM was presented to explore the influences of the heterogeneity of amygdale structure and sample size on the equivalent mechanical characteristics of basalt. The following conclusions are drawn:

(1) The SRM model, which is established by combining the DFN model generated from the statistical characteristics of the geometric parameters of amygdales and an FDEM model representing the intact matrix, can represent the meso-structural heterogeneity of the rock, and accurately reproduce the mechanical behaviours of amygdaloidal basalt observed in laboratory tests, such as failure modes and characteristics of stress-strain curve.

(2) The presence of amygdales plays a key role in controlling the mechanical characteristics of basalt. With the increase in amygdale content (quantity, size and aspect ratio), E increases linearly, while the UCS (peak strength σ_c) shows a exponential or logarithmic decay. The trends in σ_{ci}, σ_{cd} and σ_{cd}/σ_c are similar to that of σ_c, while σ_{ci}/σ_c tended to decrease significantly at first and then increased slightly.

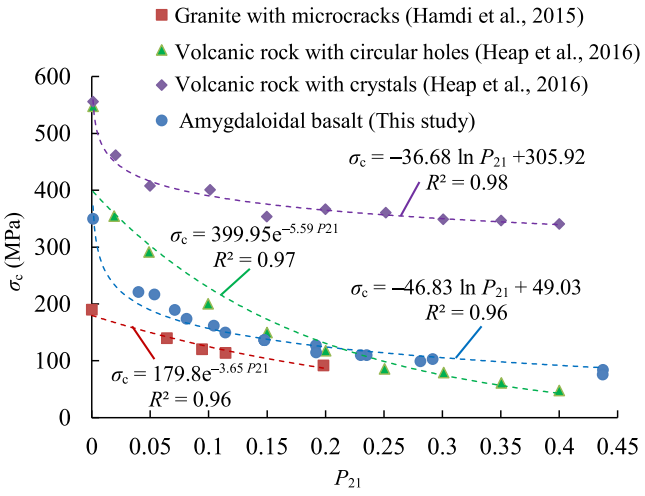

Fig. 14. Influence of defect content on σ_c.

(3) With the increase in amygdale orientation θ in the range of 0°–90°, E decreases gradually, with a maximum found when the amygdales lie parallel to the direction of loading. The UCS (peak strength σ_c), σ_{ci} and σ_{cd} first decrease and then increase, with high value at both ends and a low value in the middle; on the contrary, σ_{ci}/σ_c and σ_{cd}/σ_c first increase and then decrease, being low at both ends and high in the middle. Therefore, amygdaloidal basalt exhibits relatively significant strength and stiffness anisotropy.

(4) An REV size of 200 mm for amygdaloidal basalt blocks was determined according to the scale-dependence of mechanical and geometric characteristics. The mechanical features obtained at this scale are regarded as equivalent continuum properties and may be applied as the input parameters for the simulation of large-scale rock masses based on a continuum approach. Hence, the strength of rock obtained through laboratory tests on samples with small scales cannot be applied for the estimation of the strength of rock blocks. The REV size and strength of rock blocks could be determined through scale effect analysis.

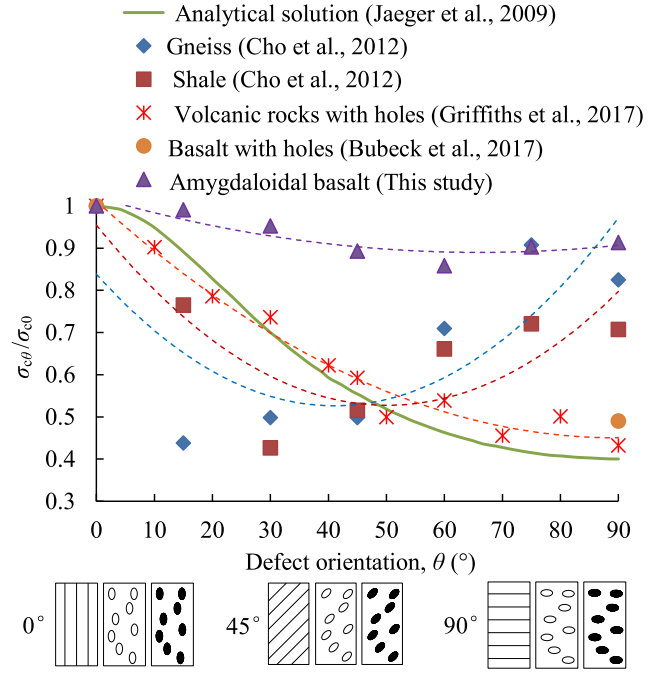

Fig. 15. Influence of defect orientation on σ_c.

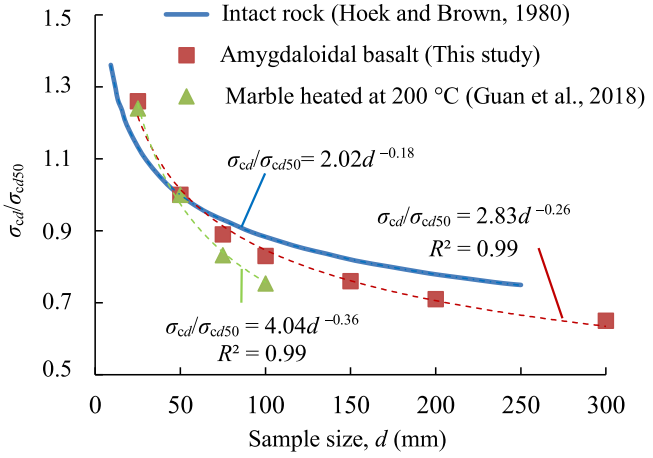

Fig. 16. Influence of sample size on σ_c.

Declaration of competing interest

The authors declare that they have no known competing financial interests or personal relationships that could have appeared to influence the work reported in this paper.

Acknowledgments

This work is supported by the Key Projects of the Yalong River Joint Fund of the National Natural Science Foundation of China (Grant No. U1865203), the Key Program of National Natural Science Foundation of China (Grant No. 41931286), and the China Postdoctoral Science Foundation (Grant No. 2021M691147). The authors also thank Geomechanica Inc. for the use of Irazu simulation software and Dr. Omid Mahabadi for his patient guidance in using the software and valuable suggestions regarding this manuscript.

List of symbols

P_{21}	Areal fracture intensity
σ_3	Confining stress
$\sigma_1-\sigma_3$	Deviatoric stress
σ_c	UCS
σ_f	Peak strength
σ_{ci}	Crack initiation strength
σ_{cd}	Crack damage strength
σ_{ci}/σ_f	Initiation strength ratio
σ_{cd}/σ_f	Damage strength ratio
ρ	Bulk density
E	Young's modulus
ν	Poisson's ratio
φ	Internal friction angle
c	Cohesion
σ_t	Tensile strength
K_{Ic}	Mode I fracture toughness
G_{f1}	Mode I fracture energy
G_{f2}	Mode II fracture energy
P_n	Normal contact penalty
P_t	Tangential contact penalty
P_f	Fracture penalty

ε_1 Axial strain
ε_3 Lateral strain

References

Abdelaziz, A., Zhao, Q., Grasselli, G., 2018. Grain based modelling of rocks using the combined finite-discrete element method. Comput. Geotech. 103, 73–81.
Aziznejad, S., Esmaieli, K., Hadjigeorgiou, J., Labrie, D., 2018. Responses of jointed rock masses subjected to impact loading. J. Rock Mech. Geotech. Eng. 10 (4), 624–634.
Bahrani, N., Kaiser, P.K., 2016. Numerical investigation of the influence of specimen size on the unconfined strength of defected rocks. Comput. Geotech. 77, 56–67.
Baud, P., Wong, T.F., Zhu, W., 2014. Effects of porosity and crack density on the compressive strength of rocks. Int. J. Rock Mech. Min. Sci. 67, 202–211.
Bubeck, A., Walker, R.J., Healy, D., Dobbs, M., Holwell, D.A., 2017. Pore geometry as a control on rock strength. Earth Planet Sci. Lett. 457, 38–48.
Cai, M., Kaiser, P.K., Tasaka, Y., Maejima, T., Morioka, H., Minami, M., 2004. Generalized crack initiation and crack damage stress thresholds of brittle rock masses near underground excavations. Int. J. Rock Mech. Min. Sci. 41 (5), 833–847.
Cao, R.H., Cao, P., Lin, H., Ma, G.W., Fan, X., Xiong, X.G., 2018. Mechanical behavior of an opening in a jointed rock-like specimen under uniaxial loading: experimental studies and particle mechanics approach. Arch. Civil. Mech. Eng. 18 (4), 198–214.
Cho, J.W., Kim, H., Jeon, S., Min, K.B., 2012. Deformation and strength anisotropy of Asan gneiss, Boryeong shale, and Yeoncheon schist. Int. J. Rock Mech. Min. Sci. 50, 158–169.
Dai, F., Li, B., Xu, N.W., Fan, Y.L., Zhang, C.Q., 2016. Deformation forecasting and stability analysis of large-scale underground powerhouse caverns from microseismic monitoring. Int. J. Rock Mech. Min. Sci. 86, 269–281.
Esmaieli, K., Hadjigeorgiou, J., Grenon, M., 2010. Estimating geometrical and mechanical REV based on synthetic rock mass models at Brunswick Mine. Int. J. Rock Mech. Min. Sci. 47 (6), 915–926.
Farahmand, K., Vazaios, I., Diederichs, M.S., Vlachopoulos, N., 2018. Investigating the scale-dependency of the geometrical and mechanical properties of a moderately jointed rock using a synthetic rock mass (SRM) approach. Comput. Geotech. 95, 162–179.
Griffiths, L., Heap, M.J., Xu, T., Chen, C.F., Baud, P., 2017. The influence of pore geometry and orientation on the strength and stiffness of porous rock. J. Struct. Geol. 96, 149–160.
Guan, R., Peng, J., Yao, M.D., Jiang, Q.H., Wong, L.N.Y., 2018. Effects of specimen size and thermal-damage on physical and mechanical behavior of a fine-grained marble. Eng. Geol. 232 (8), 46–55.
Hamdi, P., Stead, D., Elmo, D., 2015. Characterizing the influence of stress-induced microcracks on the laboratory strength and fracture development in brittle rocks using a finite-discrete element method-micro discrete fracture network FDEM-μDFN approach. J. Rock Mech. Geotech. Eng. 7 (6), 609–625.
Heap, M.J., Wadsworth, F.B., Xu, T., Chen, C.F., Tang, C.A., 2016. The strength of heterogeneous volcanic rocks: a 2D approximation. J. Volcanol. Geoth. Res. 319, 1–11.
Hoek, E., Brown, E.T., 1980. Underground Excavations in Rock. Institution of Mining and Metallurgy, London, UK.
Hoek, E., Martin, C.D., 2014. Fracture initiation and propagation in intact rock - a review. J. Rock Mech. Geotech. Eng. 6 (4), 287–300.
Jin, J., Cao, P., Chen, Y., Pu, C.Z., Mao, D.W., Fan, X., 2017. Influence of single flaw on the failure process and energy mechanics of rock-like material. Comput. Geotech. 86, 150–162.
Lei, Q.H., Latham, J.P., Xiang, J.S., Tsang, C.F., 2017. Role of natural fractures in damage evolution around tunnel excavation in fractured rocks. Eng. Geol. 231, 100–113.
Lisjak, A., Grasselli, G., 2014. A review of discrete modeling techniques for fracturing processes in discontinuous rock masses. J. Rock Mech. Geotech. Eng. 6 (4), 301–314.
Liu, G., Cai, M., Huang, M., 2018. Mechanical properties of brittle rock governed by micro-geometric heterogeneity. Comput. Geotech. 104, 358–372.
Liu, N., Zhang, C.S., Chu, W.J., 2012. Fracture characteristics and damage evolution law of Jinping deep marble. Chin. J. Rock Mech. Eng. 31 (8), 1606–1613 (in Chinese).
Liu, Z.J., Zhang, C.Q., Zhang, C.S., Gao, Y., Zhou, H., Chang, Z.R., 2019. Deformation and failure characteristics and fracture evolution of cryptocrystalline basalt. J. Rock Mech. Geotech. Eng. 11 (5), 990–1003.
Mahabadi, O.K., Grasselli, G., Munjiza, A., 2010. Y-GUI: a graphical user interface and pre-processor for the combined finite-discrete element code, Y2D, incorporating material heterogeneity. Comput. Geotech. 36 (2), 241–252.
Martin, C.D., Chandler, N.A., 1994. The progressive fracture of Lac du Bonnet granite. Int. J. Rock Mech. Min. Sci. 31 (6), 643–659.
Moosavi, S., Scholtès, L., Giot, R., 2018. Influence of stress induced microcracks on the tensile fracture behavior of rocks. Comput. Geotech. 104, 81–95.
Munjiza, A., 2004. The Combined Finite-Discrete Element Method. John Wiley & Sons, London, UK.
Shaunik, D., Singh, M., 2019. Strength behaviour of a model rock intersected by non-persistent joint. J. Rock Mech. Geotech. Eng. 11 (6), 1243–1255.
Stavroua, A., Murph, W., 2018. Quantifying the effects of scale and heterogeneity on the confined strength of micro-defected rocks. Int. J. Rock Mech. Min. Sci. 102, 131–143.
Vazaios, I., Farahmand, K., Vlachopoulos, N., Diederichs, M.S., 2018. Effects of confinement on rock mass modulus: a synthetic rock mass modelling (SRM) study. J. Rock Mech. Geotech. Eng. 10 (3), 436–456.
Vöge, M., Lato, M.J., Diederichs, M.S., 2013. Automated rockmass discontinuity mapping from 3-dimensional surface data. Eng. Geol. 164, 155–162.
Wang, X., Cai, M., 2019. A comprehensive parametric study of grain-based models for rock failure process simulation. Int. J. Rock Mech. Min. Sci. 115, 60–76.
Wang, Y.L., Tang, J.X., Dai, Z.Y., Yi, T., 2018. Experimental study on mechanical properties and failure modes of low-strength rock samples containing different fissures under uniaxial compression. Eng. Fract. Mech. 197, 1–20.
Xia, Y.J., Zhang, C.Q., Zhou, H., Chen, J.L., Gao, Y., Liu, N., Chen, P.Z., 2019. Structural characteristics of Baihetan columnar jointed basalt in drainage tunnel of Baihetan hydropower station and its influence on the behavior of acoustic P-wave anisotropy. Eng. Geol. 264, 105304.
Yan, C.Z., Jiao, Y.Y., Zheng, H., 2018. A fully coupled three-dimensional hydro-mechanical finite discrete element approach with real porous seepage for simulating 3D hydraulic fracturing. Comput. Geotech. 96, 73–89.
Yang, S.Q., Tian, W.L., Huang, Y.H., 2018. Failure mechanical behavior of pre-holed granite specimens after elevated temperature treatment by particle flow code. Geothermics 72, 124–137.
Yang, T., Liu, H.Y., Tang, C.A., 2017. Scale effect in macroscopic permeability of jointed rock mass using a coupled stress-damage-flow method. Eng. Geol. 228 (13), 121–136.
Zhang, C.Q., Liu, Z.J., Pan, Y.B., Gao, Y., Zhou, H., Cui, G.J., 2020. Influence of amygdale on crack evolution and failure behavior of basalt. Eng. Fract. Mech. 226, 106843.
Zhang, S., Tang, H.M., Zhan, H.B., Lei, G.P., Cheng, H., 2015. Investigation of scale effect of numerical unconfined compression strengths of virtual colluvial–deluvial soil–rock mixture. Int. J. Rock Mech. Min. Sci. 77, 208–219.
Zhang, W., Chen, J.P., Cao, Z.X., Wang, R.Y., 2013. Size effect of RQD and generalized representative volume elements: a case study on an underground excavation in Baihetan dam, Southwest China. Tunn. Undergr. Space Technol. 35, 89–98.
Zhao, X.G., Cai, M., Wang, J., Li, P.F., Ma, L.K., 2015. Objective determination of crack Initiation stress of brittle rocks under compression using AE measurement. Rock Mech. Rock Eng. 48 (6), 2473–2484.
Zhou, B., Wang, J., Wang, H., 2018a. Three-dimensional sphericity, roundness and fractal dimension of sand particles. Geotechnique 68 (1), 18–30.
Zhou, B., Wei, D.H., Ku, Q., Wang, J.F., Zhang, A.J., 2020. Study on the effect of particle morphology on single particle breakage using a combined finite-discrete element method. Comput. Geotech. 122, 103532.
Zhou, X.P., Lian, Y.J., Wong, L.N.Y., Berto, F., 2018b. Understanding the fracture behavior of brittle and ductile multi-flawed rocks by uniaxial loading by digital image correlation. Eng. Fract. Mech. 199, 438–460.
Zong, Y.J., Han, L.J., Wei, J.J., Wen, S.Y., 2016. Mechanical and damage evolution properties of sandstone under triaxial compression. Int. J. Rock Mech. Min. Sci. 26 (4), 601–607.

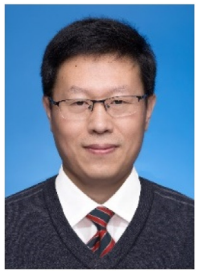

Dr. Chuanqing Zhang is a professor at Institute of Rock and Soil Mechanics, Chinese Academy of Sciences (CAS). He is a member of editorial board of *Rock and Soil Mechanics*, and a member of Chinese Society for Rock Mechanics and Engineering (CSRME) and International Society for Rock Mechanics and Rock Engineering (ISRM). He is one of first group members and outstanding members of Youth Innovation Promotion Association, CAS, and is the winner of the 9th Youth Science and Technology Gold Award of CSRME. His research interests focus on the rock mechanics, disaster control and fault activation in deep underground engineering. In recent years, Dr. Zhang has chaired one of the Key Projects of the Yalong River Joint Fund of the National Natural Science Foundation of China, hosted and participated in 11 projects funded by national, provincial and ministerial projects. He has provided consultation for more than 20 national major projects and carried out systematic research on rock mechanics problems encountered in these projects. The research results have been widely applied in the construction process of these projects and played an important role in ensuring the safety of projects.